Acta Crystallographica Section D
Biological Crystallography
ISSN 0907-4449

The effect of heavy atoms on the conformation of the active-site polypeptide loop in human ABO(H) blood-group glycosyltransferase B

James A. Letts,[a] Mattias Persson,[b] Brock Schuman,[a] Svetlana N. Borisova,[a] Monica M. Palcic[b] and Stephen V. Evans[a]*

[a]The Department of Biochemistry and Microbiology, University of Victoria, Victoria, British Columbia, V8W 3P6, Canada, and [b]The Carlsberg Laboratory, Gamle Carlsberg Vej 10, 2500 Valby, Copenhagen, Denmark

Correspondence e-mail: svevans@uvic.ca

Received 16 March 2007
Accepted 31 May 2007

PDB References: GTB C209A, 2pgv, r2pgvsf; 2pgy, r2pgysf.

The human ABO(H) blood-group antigens are oligosaccharide structures that are expressed on erythrocyte and other cell surfaces. The terminal carbohydrate residue differs between the blood types and determines the immune reactivity of this antigen. Individuals with blood type A have a terminal *N*-acetylgalactosamine residue and those with blood type B have a terminal galactose residue. The attachment of these terminal carbohydrates are catalyzed by two different glycosyltransferases: an $\alpha(1\rightarrow3)$*N*-acetylgalactosaminyltransferase (GTA) and an $\alpha(1\rightarrow3)$galactosyltransferase (GTB) for blood types A and B, respectively. GTA and GTB are homologous enzymes that differ in only four of 354 amino-acid residues (Arg/Gly176, Gly/Ser235, Leu/Met266 and Gly/Ala268 in GTA and GTB, respectively). Diffraction-quality crystals of GTA and GTB have previously been grown from as little as 10 mg ml^{-1} stock solutions in the presence of Hg, while diffraction-quality crystals of the native enzymes require much higher concentrations of protein. The structure of a single mutant C209A has been determined in the presence and absence of heavy atoms and reveals that when mercury is complexed with Cys209 it forces a significant level of disorder in a polypeptide loop (amino acids 179–195) that is known to cover the active site of the enzyme. The observation that the more highly disordered structure is more amenable to crystallization is surprising and the derivative provides insight into the mobility of this polypeptide loop compared with homologous enzymes.

1. Introduction

Glycosyltransferases are ubiquitous enzymes that catalyze the transfer of monosaccharides from nucleotide-sugar donors to carbohydrate, protein, lipid or nucleic acid acceptors. These enzymes are responsible for the generation of simple and complex oligosaccharides and polysaccharides as well as glycoconjugates such as glycoproteins and glycolipids. Many pathogenic organisms express an assortment of glycosyltransferases whose products contribute to virulence and which are potential targets for a new class of therapeutics to treat bacterial (Lazar & Walker, 2002) and fungal infections (Liu & Balasubramanian, 2001). Furthermore, glycosyltransferases have been suggested as therapeutic targets for other human disorders such as diabetes (Somsak *et al.*, 2003). Unfortunately, there is a paucity of structural data for glycosyltransferases in general, with known examples in only 28 of 87 families (CAZy; Coutinho & Henrissat, 1999; Coutinho *et al.*, 2003), and three-dimensional studies are in their infancy.

The human blood-group glycosyltransferases GTA and GTB are prototypic retaining glycosyltransferases and are model probes of this class of enzyme. They are the two most homologous naturally occurring glycosyltransferase enzymes known to specifically transfer distinct naturally occurring donors and differ only in four of 354 amino-acid residues: Arg/Gly176, Gly/Ser235, Leu/Met266 and Gly/Ala268 (Yamamoto *et al.*, 1990).

GTA and GTB synthesize their specific antigens by the respective transfer of GalNAc from UDP-GalNAc for GTA and Gal from UDP-Gal for GTB to their common acceptor, the H-antigen disaccharide α-L-Fuc*p*-(1$\rightarrow$2)-β-D-Gal*p*-*OR*, where *R* is a glycoprotein or glycolipid. Individuals with the gene for GTA have blood group A, those with the gene for GTB have blood group B, those with genes for both enzymes or a *cis*-acting enzyme (Yazer *et al.*, 2006) have blood type AB and those with an untranslated or mutated inactive form of the enzyme have blood group O. The ABO(H) blood-group antigen plays a major role in tissue-graft rejection and is the major cause of blood-transfusion mismatch (Fressy, 1992).

The first structures of GTA and GTB were obtained as mercury derivatives (Patenaude *et al.*, 2002) and revealed that donor recognition could only be significantly influenced by Leu/Met266 and Gly/Ala268 (Seto *et al.*, 1999). The remaining two critical residues, Arg/Gly176 and Gly/Ser235, were known to have little effect on donor specificity and were located at the periphery of the active site. This structure also revealed two completely disordered regions of polypeptide chain: a 16-residue internal loop (amino-acid residues 179–195) near the active site and the ten carboxy-terminal residues (amino acids 345–354).

Disordered loops are a common structural feature of glycosyltransferases and are known to be important in the catalytic activity (Qasba *et al.*, 2005; Yazer & Palcic, 2005). Although the exact locations of the disordered loops differ among glycosyltransferases, they are usually proximal to the active site. The disordered loop has been observed to become ordered for several glycosyltransferase structures in going from unliganded to donor-bound states (Chiu *et al.*, 2004; Qasba *et al.*, 2005; Unligil *et al.*, 2000).

The mercury derivatives of GTA and GTB have not been observed to crystallize in the donor-bound state and the disordered loop proximal to the active site displays the same level of disorder whether bound to UDP and Mn^{II} or in the absence of ligands. In order to evaluate the effect of mercury coordination to Cys209 adjacent to the disordered loop, to Cys284 distant from the loop and to the structure of the enzyme in general, we expressed the GTB C209A mutant enzyme and crystallized it in the presence and absence of mercury.

2. Materials and methods

2.1. Generation of mutant protein

Site-directed mutagenesis was carried out using the QuikChange II XL Site-Directed Mutagenesis Kit (Stratagene). PCR was performed in a Peltier Thermal PTC-200 thermocycler (Bio-Rad, CA, USA). The plasmid vector pCWΔlac harbouring the $-$10GTB (amino acids 63–354) gene was used as template. The PCR cycling conditions were initial denaturation at 368 K for 35 s followed by 18 cycles at 368 K for 30 s, 333 K for 60 s, 341 K for 10 min and a final extension at 341 K for 10 min. The primers used for mutagenesis were as follows: C209Asense, 5′-CC GAA GTT GAC TAC CTG GTT **GCT** GTT GAC GTT GAC ATG GAG TTC C-3′; C209Aantisense, 5′-G GAA CTC CAT GTC AAG GTC AAC **AGC** AAC CAG GTA GTC AAC TTC GG-3′. The altered nucleotides are shown in bold. To digest template-methylated nonmutated plasmid DNA, the PCR reaction mixture was treated with 1 µl *Dpn*I (10 U µl^{-1}) for 60 min at 310 K. The *Dpn*I-treated plasmids were transformed into *Escherichia coli* XL10-Gold and sequencing was performed by Agowa (Berlin, Germany). Positive mutants were transformed into *E. coli* BL21 Gold cells for expression. GTB C209A purified using a two-step protocol using ion-exchange chromatography followed by UDP-hexanolamine affinity chromatography was assayed and kinetically characterized as described previously (Seto *et al.*, 1999; Marcus *et al.*, 2003). The k_{cat} (6.8 s^{-1}) for GTB C209A is greater than that for GTB (4.9 s^{-1}), while the K_m values for the UDP-Gal donor (188 µ*M*) and the α-L-Fuc*p*-(1$\rightarrow$2)-β-D-Gal*p*-*O*(CH$_2$)$_7$CH$_3$ acceptor (174 µ*M*) are somewhat higher than those of GTB (K_m is 27 µ*M* for the donor and 88 µ*M* for the acceptor; Marcus *et al.*, 2003).

2.2. Crystallography

GTB C209A was crystallized in both the presence and the absence of mercury. Crystals grown in the presence of mercury used conditions corresponding to the original report of the structures of the GTB enzyme (Patenaude *et al.*, 2002): 10 µl drops containing 6–8 mg ml^{-1} GTB, 70 m*M* *N*-(2-acetamido)-2-iminodiacetic acid (ADA) pH 7.5, 50 m*M* sodium acetate pH 4.6, 40 m*M* NaCl, 5–8 m*M* $MnCl_2$, 2.5%(*v*/*v*) 2-methyl-2,4-pentanediol (MPD), 5%(*v*/*v*) glycerol, 2%(*w*/*v*) PEG 4000 and 0.3–0.5 m*M* 3-chloromercuri-2-methoxypropylurea suspended over 1 ml reservoir solution [50 m*M* ADA pH 7.5, 10 m*M* $MnCl_2$, 100 m*M* ammonium sulfate, 5%(*v*/*v*) MPD, 10%(*v*/*v*) glycerol and 8–10%(*w*/*v*) PEG 4000]. Exhaustive attempts to grow crystals of native GTB in the absence of mercury using protein concentrations of 6–8 mg ml^{-1} were unsuccessful. Crystals of the C209A mutant were first grown from protein concentrations of >30 mg ml^{-1}, with the lowest observed concentration that yielded diffraction-quality crystals being 15 mg ml^{-1}. 5–8 µl drops containing 1% PEG 4000, 4.5% MPD, 0.1 *M* ammonium sulfate, 0.07 *M* NaCl, 0.05 *M* ADA pH 7.5 and 5 m*M* $CoCl_2$ were stored at 277–279 K for 3–5 d over a reservoir of 2.7% PEG 4000, 7% MPD, 0.32 *M* ammonium sulfate, 0.25 *M* NaCl and 0.2 *M* ADA. Both sets of crystals were washed with mother liquor containing 6–7% PEG 4000, 70 m*M* ADA pH 7.5, 30 m*M* sodium acetate pH 4.6, 40 m*M* ammonium sulfate, 29–30% glycerol and 9–10 m*M* $MnCl_2$ or 5 m*M* $CoCl_2$ for the heavy-metal derivative or native protein, respectively.

Table 1
Data-collection and refinement statistics for GTB C209A.

Values in parentheses are for the highest resolution shell.

	With Hg	Without Hg
Resolution (Å)	20–1.79	20–2.39
Space group	$C222_1$	$C222_1$
Unit-cell parameters (Å)		
a	52.50	53.39
b	149.26	151.85
c	78.43	80.24
R_{merge}† (%)	4.9 (31.1)	7.5 (27.3)
Completeness (%)	93.5 (89.1)	96.0 (95.6)
Unique reflections	27550	12772
Refinement		
R_{work}‡ (%)	18.6	16.8
R_{free}‡§ (%)	21.3	23.9
No. of waters	200	119
R.m.s.d. bonds (Å)	0.015	0.012
R.m.s.d. angles (°)	1.44	1.34
Ramachandran, residues in disallowed regions	0	0
PDB code	2pgv	2pgy

† $R_{merge} = \sum|I_{obs} - I_{ave}|/\sum I_{ave}$. ‡ $R_{work} = \sum||F_o| - |F_c||/\sum|F_o|$. § 10% of reflections were omitted for R_{free} calculations.

Data were collected on a Rigaku R-AXIS IV^{++} area detector at a crystal-to detector distance of 72 mm and with exposure times of between 4.0 and 5.0 min for 0.5° oscillations and were processed using *d*TREK* (Pflugrath, 1999). X-rays were produced using an MM-002 generator (Rigaku/MSC) coupled to Osmic Blue confocal X-ray mirrors with a power level of 30 W (Osmic). The crystal was frozen and maintained under cryogenic conditions at a temperature of 113 K using a CryoStream 700 crystal cooler (Oxford Cryosystems). For completeness, structures were solved using molecular-replacement techniques (*MOLREP*; Vagin & Teplyakov, 1997) with wild-type GTB (PDB code 1lz7) as a starting model and a single outstanding solution was found in both cases. Subsequent refinement was performed using *REFMAC*5 (Murshudov *et al.*, 1997) in the *CCP*4 program suite (Collaborative Computational Project, Number 4, 1994). Superimpositions were also calculated using *CCP*4. Figs. 1 and 5 were generated using *SETOR* (Evans, 1993) and Figs. 2 and 3 were generated using *SETORIBBON* (unpublished program).

3. Results and discussion

3.1. Structural overview

Details of the data-collection and refinement results for GTB C209A in the presence and absence of mercury are shown in Table 1. Diffraction data were collected to maximum resolutions of 1.79 and 2.39 Å, with final R_{work} values of 18.0% and 16.8% and R_{free} values of 21.2% and 23.9%, for the heavy-atom and native forms, respectively. Crystals of GTB C209A grown in the presence of mercury show Hg bound to Cys284 as do the crystals of GTB. The structures show excellent electron density along the entire length of the polypeptide chain, with the exception of residues 177–187 and the ten carboxy-terminal amino-acid residues, both of which are also disordered in the native GTB structure (Patenaude *et al.*, 2002). However, eight of the amino-acid residues that are disordered in the heavy-atom wild-type crystals (residues 188–195) are ordered in the crystals of GTB C209A grown both in the presence and in the absence of mercury (Fig. 1). Electron density for the newly ordered amino-acid residues that result from the mutation of Cys209 to alanine is shown in Fig. 2. Well defined main-chain density is observed for all of the residues in this now ordered region, with the exception of Asp194. The side chains of the amino-acid residues exposed to solvent are disordered (Glu190, Met191, Asp194 and Phe195), whereas the side chains of the amino-acid residues buried in the protein surface are well ordered (Arg188, Met189, Ile192 and Ser193). This trend continues with the side chain of Cys196 being ordered and the side chains of Asp197 and Arg198 being disordered. The now ordered amino-acid residues 188–195 form a helical structure, with residues 188–194 making two turns of an α-helix which is interrupted at residue 196 by an 85° bend followed by another short α-helix comprised of residues 197–203. The effect of mercury derivatization on the conditions required to obtain diffraction-quality crystals was surprising given that neither

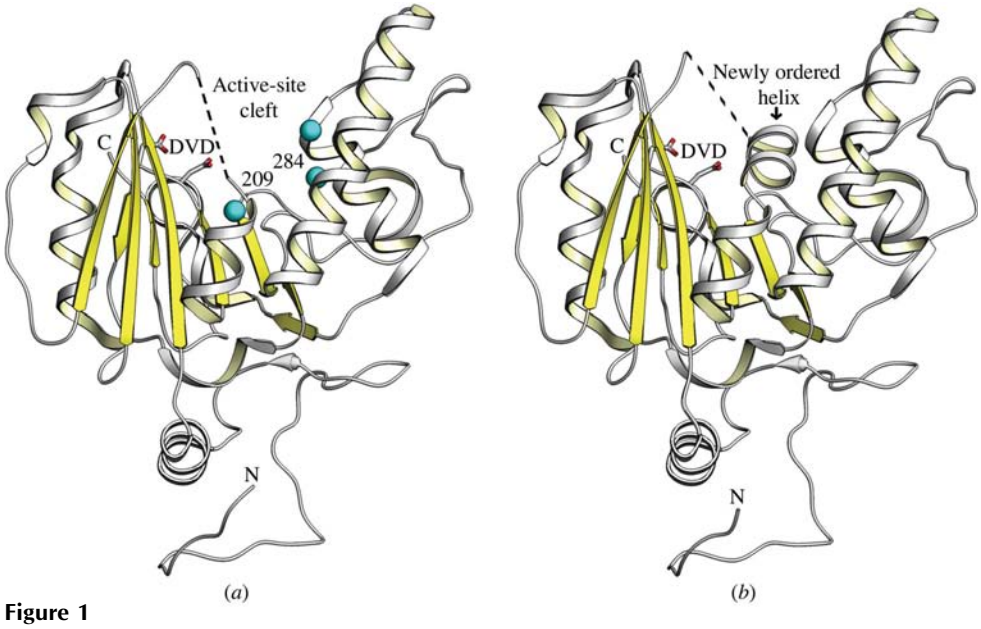

Figure 1
Ribbon diagrams of GTB (*a*) and GTB C209A (*b*) showing the position of the mercury-binding sites in GTB and the newly ordered helix in GTB C209A. The mercury-binding sites are labelled with the residue number of the cysteine to which they coordinate. Also shown is the DVD motif which forms the nucleotide donor-binding site. Hg atoms are shown as cyan spheres. The side chains of Asp211 and Asp213 of the DVD are coloured by atom, with oxygen red and carbon white.

the Hg atoms nor any of the residues surrounding them were involved in crystal contacts.

3.2. Mercury does not affect the conformation of active-site residues

The structures of the mercury derivative of GTB (Patenaude *et al.*, 2002) and of native GTB C209A were superimposed using least-squares methods. Neither the residues that are involved in acceptor recognition (His233, Ser235, Thr245, Trp300, Glu303 and Asp326) nor those that are involved in donor recognition (Asp211 and 213 of the DVD motif, Met266 and Ala268 that are important for differentiating between the A and B donors) change their relative configuration. Superimposition of wild-type GTB with GTB C209A using the C^{α} atoms of residues 63–176 and 196–345 gave an r.m.s. (root-mean-square) deviation of 0.36 Å. Superimposition using all atoms of the active-site residues gives an r.m.s. displacement of 0.22 Å.

3.3. The effect of mercury on disorder

The structure of GTB C209A demonstrates that the mercury coordinated by Cys209 is partially responsible for the disorder of the 16-amino-acid internal loop observed in the heavy-atom structure of GTB (Patenaude *et al.*, 2002). The mercury ion that is coordinated by Cys209 in wild-type GTB occupies the same position as the side chain of Ile192 in the internal loop that is ordered by the mutation of Cys209 to alanine (Fig. 3*a*). In the GTB C209A structure, mercury is absent from the region around residue 209 and this portion of the loop is able to order.

Mercury is observed coordinated to Cys284 in both the wild-type and GTB C209A derivatives. This cysteine residue adopts multiple conformations bound to two partially occupied mercury ions (Figs. 3*b* and 3*c*). Although the newly ordered residue Met189 occupies the same space as one of these mercury ions, they do not appear to affect the conformation of the loop as the mercury derivative and native structure of GTB C209A show the same level of ordering.

3.4. Comparison of GTB C209A with α3GT

The closest mammalian counterpart of GTA and GTB of known structure is bovine $\alpha(1\rightarrow3)$galatosyltransferase (α3GT), which shares 45% sequence identity (Gastinel *et al.*, 2001; Fig. 3). Bovine α3GT is also a retaining family GT-6 glycosyltransferase with a GT-A fold and catalyzes the transfer of Gal from UDP-Gal to oligosaccharides ending in LacNAc [β-D-Gal-$(1\rightarrow4)$-β-D-GlcNAc]. Interestingly, unlike GTA and GTB, the structure of α3GT displays no disordered internal loop.

The disordered region in wild-type GTB (amino acids 177–195) corresponds to α-helix 4 in α3GT (amino acids 194–213), which forms part of the active-site cleft and UDP-Gal binding site (Figs. 4 and 5*b*). Amino-acid residues Ser199 and Arg202 of α-helix 4 in α3GT have been postulated to contact the donor sugar (Boix *et al.*, 2002). In GTB the equivalent residues are Ser185 and Arg188, which are disordered in the wild-type GTB crystal structure. However, in the crystal structure of GTB C209A Arg188 is ordered and shows a similar orientation to that of Arg202 in α3GT (Figs. 5*a* and 5*b*). Therefore, as predicted by modelling, this region of both enzymes is likely to be important for donor recognition (Heissigerova *et al.*, 2003).

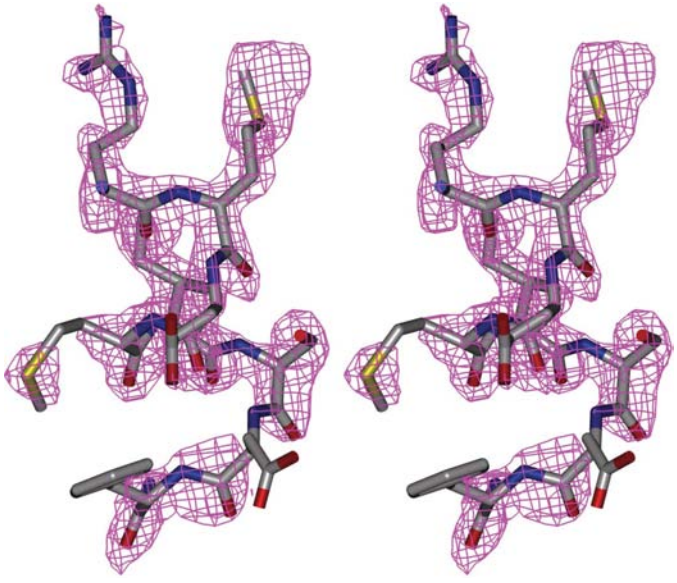

Figure 2
Stereo image of the electron density ($2|F_o| - |F_c|$) of the newly ordered amino-acid residues Arg188 (top) to Phe195 (bottom) of GTB C209A crystallized in the presence of Hg. Electron density was contoured at 1.00σ. Atoms are coloured by element, with carbon white, nitrogen blue, oxygen red and sulfur yellow.

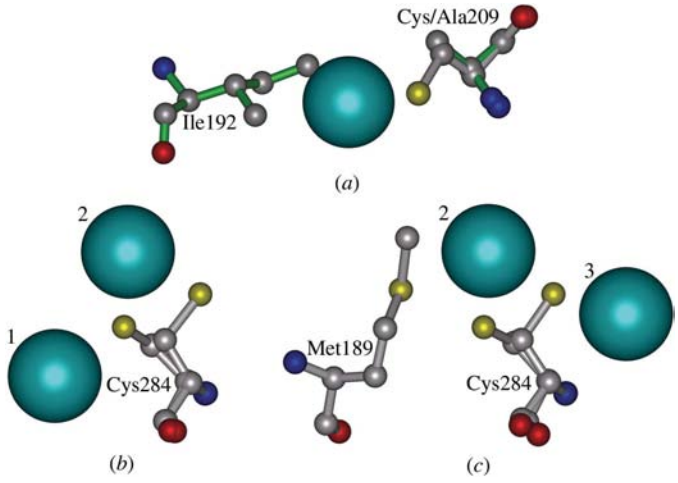

Figure 3
(*a*) Mutation-site superimposition of wild-type GTB (silver bonds) and GTB C209A (green bonds), showing the conflict in position between the mercury (cyan sphere) coordinated to Cys209 in wild-type GTB and the position of the newly ordered Ile192 in GTB C209A. (*b*) and (*c*) Amino-acid residue Cys284 in wild-type GTB (*b*) and GTB C209A (*c*), showing the alteration in the coordination of mercury ions resulting from the ordering of amino-acid residue Met189. Atoms are coloured by element, with carbon silver, nitrogen blue, oxygen red, sulfur yellow and mercury cyan.

```
α3GT:   94  RPEVVTMTKWKAPVVWEGTYNRAVLDNYYAKQKITVGLTVFAVGRYIEHYLEEFLTSANK 153
            R +V+ +T W AP+VWEGT+N  +L+  +  Q  T+GLTVFA+ +Y+  +L+ FL +A K
GTB:    81  RKDVLVVTPWLAPIVWEGTFNIDILNEQFRLQNTTIGLTVFAIKKYVA-FLKLFLETAEK 139

α3GT:   154 HFMVGHPVIFYIMVDDVSRMPLIELGPLRSFKVFKIKPEKRWQDISMMRMKTIGEHIVAH 213
            HFMVGH V +Y+  D  + +P + LG  R   V ++   KRWQD+SM RM+ I + ▼  ▲
GTB:    140 HFMVGHRVHYYVFTDQPAAVPRVTLGTGRQLSVLEVGAYKRWQDVSMRRMEMISDFCERR 199

α3GT:   214 IQHEVDFLFCMDVDQVFQDKFGVETLGESVAQLQAWWYKADPNDFTYERRKESAAYIPFG 273
               EVD+L C+DVD  F+D  GVE L      L   +Y +    FTYERR +S AYIP
GTB:    200 FLSEVDYLVCVDVDMEFRDHVGVEILTPLFGTLHPSFYGSSREAFTYERRPQSQAYIPKD 259

α3GT:   274 EGDFYYHAAIFGGTPTQVLNITQECFKGILKDKKNDIEAQWHDESHLNKYFLLNKPTKIL 333
            EGDFYY  A FGG+  +V  +T+ C + ++ D+ N IEA WHDESHLNKY L +KPTK+L
GTB:    260 EGDFYYMGRFFGGSVQEVQRLTRACHQAMMVDQANGIEAVWHDESHLNKYLLRHKPTKVL 319

α3GT:   334 SPEYCWDYH-IGLPADIKLVKMSWQTKEYNVVRNNV 368
            SPEY WD   +G PA ++ ++ +   K +  VRN
GTB:    320 SPEYLWDQQLLGWPAVLRKLRFTAVPKNHQAVRNP 354
```

Figure 4
Sequence alignment of α3GT and GTB (using *BLAST*2 sequences; Tatusova & Madden, 1999). Critical residues of GTB are highlighted in red. Disordered loops of wild-type GTB are boxed in blue. The residues that are ordered by the Cys209-to-alanine mutation are in bold. The residue at which helix 4 bends in GTB C209A and α3GT is indicated by a red triangle. The amino-acid residue differences that impact the disordered internal loop of wild-type GTB are highlighted in green. Cys209 is highlighted in yellow.

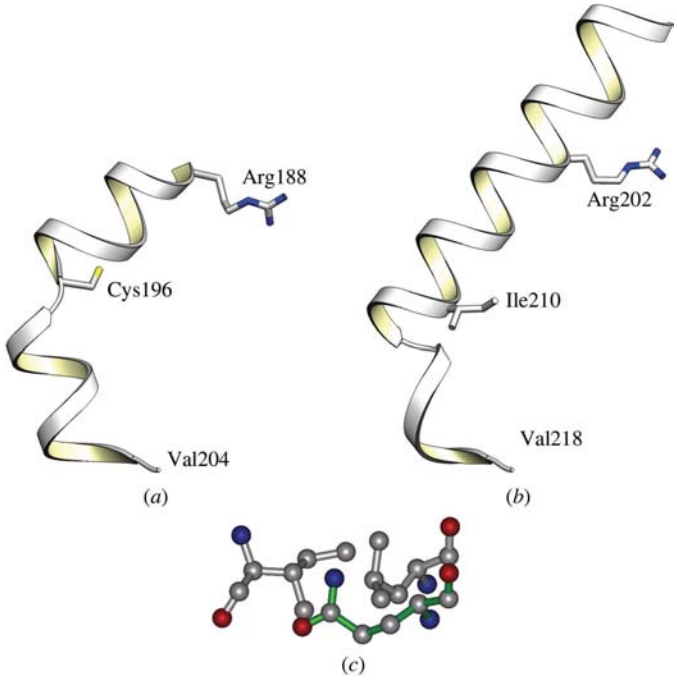

Figure 5
(*a*) Amino-acid residues 188–204 in GTB C209A, demonstrating that the newly ordered residues form an α-helix followed by a sharp bend and another short α-helix. (*b*) Amino-acid residues 195–218 of the equivalent region in α3GT. (*c*) Superimposition of GTB (green bonds) and α3GT (silver bonds), showing that the position of Gln278 conflicts with the α-helical position of Ile210, resulting in a shorter helix in GTB relative to α3GT. Atoms are coloured by element, with carbon silver, nitrogen blue, oxygen red and sulfur yellow.

In GTB C209A the newly ordered residues adopt an α-helical conformation corresponding to the C-terminal end of α-helix 4 in α3GT. In both enzymes this α-helix is followed by a sharp 85° bend and then another short helix (Figs. 5*a* and 5*b*). However, the amino-acid position at which this bend occurs differs. In α3GT the bend occurs at His213, which corresponds to Arg199 in GTB, while in GTB the bend occurs at Cys196, which corresponds to Ile210 in α3GT (Fig. 4). Therefore, α-helix 4 of α3GT is three amino acids longer at the C-terminus than the corresponding helix in GTB and the short post-bend helix is three amino-acid residues shorter at the N-terminus in α3GT (Figs. 5*a* and 5*b*). The reason for the earlier disruption of the newly ordered helix in GTB can be understood by observing the residues that it packs against. When the structures of GTB C209A and α3GT are superimposed, the position of Gln278 in GTB clashes with the position of Ile210 in α3GT, indicating that Cys196 in GTB is sterically blocked from adopting the dihedral angles necessary for continuation of the α-helix (Fig. 5*c*). The corresponding residue to Gln278 in α3GT is Leu292, which does not block Ile210 from adopting the necessary α-helical dihedral angles, allowing the helix to continue. The side-chain amide of Gln278 in GTB C209A forms a hydrogen bond to the main-chain carbonyl of Ile192 at the C-terminus of the newly ordered helix. This in essence replaces the main-chain α-helical hydrogen bond, disrupting the α-helix. In α3GT, Leu292 is incapable of forming this disruptive hydrogen bond and therefore the α-helix continues.

Given the high sequence identity of the N-terminal residues of the disordered internal loop between GTB and α-helix 4 of α3GT (Fig. 4), one would expect that this region would also continue as an α-helix in the fully closed conformation of GTB (Fig. 4). However, unlike the C-terminal residues of the disordered internal loop of GTB, the N-terminal residues are not ordered in the structure of GTB C209A. This suggests that the amino-acid differences between GTB and α3GT both in the loop and adjacent to the loop act to destabilize the N-terminal region of the loop in GTB.

The only two amino-acid differences in this region are Val184/Ile198 and Arg187/Met201 in GTB and α3GT, respectively. It has been shown by mutational studies that replacing isoleucine with valine in the core of an α-helix is destabilizing by approximately 0.8 kJ mol^{-1} (Fersht, 1999) and results from the greater hydrophobic surface area buried by the adjacent amino-acid residues in the helix. Therefore, the amino-acid difference Val184/Ile198 between GTB and α3GT, respectively, would indicate a more flexible helix in GTB.

The amino-acid substitution methionine to arginine within the core of an α-helix has been shown to not significantly alter the stability of the helix (Fersht, 1999) and so the Arg187/Met201 difference between the two enzymes would not be significant. However, both GTB and α3GT have a lysine residue and an arginine residue at the N-terminus of this region (Lys179/193 and Arg180/194 in GTB and α3GT,

respectively), which are known to destabilize α-helical structure by unfavourable interaction with the helix dipole (Fersht, 1999). When the structures of GTB and α3GT are superimposed, the positions of these positively charged residues in α3GT approach another positively charged residue (Lys124) in GTB. Therefore, in GTB the unfavourable interaction of Lys179 and Arg180 with the helix dipole would be exasperated by the proximity of Lys124. In α3GT the equivalent residue to Lys124 is Gly137, which cannot interfere with the stability of Lys193 or Arg194. This unfavourable like-charge interaction would tend to destabilize the N-terminus of this loop region in GTB relative to the equivalent α-helical region of α3GT.

4. Conclusions

The disordered internal loop observed in the structure of the human ABO(H) blood-group glycosyltransferase GTB is partially an artifact of the presence of mercury in the crystallization conditions and partially arises from inherent flexibility. The mutation of Cys209 to alanine removes a coordination site for a mercury ion, allowing a portion of this loop to adopt an ordered conformation that is similar to the conformation of the equivalent region of the homologous bovine enzyme α3GT. The differences observed in the conformation of this region between GTB and α3GT can be rationalized by examining the amino-acid differences between the two glycosyltransferases both in the loop and adjacent to it.

We would like to thank Cory Brooks and Javier Alfaro for helpful discussions. This work was supported by funding from the Canadian Institutes of Health Research and the Michael Smith Foundation for Health Research (SVE) and the Danish Natural Science Research Council (MMP). SVE is the recipient of a senior scholarship from the Michael Smith Foundation for Health Research.

References

Boix, E., Zhang, Y., Swaminathan, G. J., Brew, K. & Acharya, K. R. (2002). *J. Biol. Chem.* **277**, 28310–28318.

Chiu, C. P., Watts, A. G., Lairson, L. L., Gilbert, M., Lim, D., Wakarchuk, W. W., Withers, S. G. & Strynadka, N. C. (2004). *Nature Struct. Mol. Biol.* **11**, 163–170.

Collaborative Computational Project, Number 4 (1994). *Acta Cryst.* D**50**,760–763.

Coutinho, P. M., Deleury, E., Davies, G. J. & Henrissat, G. (2003). *J. Mol. Biol.* **328**, 307–317.

Coutinho, P. M. & Henrissat, B. (1999). *Recent Advances in Carbohydrate Bioengineering*, edited by H. J. Gilbert, G. Davies, B. Henrissat & B. Svensson, pp. 3–12. Cambridge: The Royal Society of Chemistry.

Evans, S. V. (1993). *J. Mol. Graph.* **11**, 134–138.

Fersht, A. (1999). *Structure and Mechanism in Protein Science: A Guide to Enzyme Catalysis and Protein Folding*, 1st Ed. Cambridge: W. H. Freeman & Co..

Fressy, P. (1992). *Rev. Fr. Transf. Hemobiol.* **35**, 363–377.

Gastinel, L. N., Bignon, C., Misra, A. K., Hindsgual, O., Shaper, J. H. & Joziasse, D. H. (2001). *EMBO J.* **20**, 638–649.

Heissigerova, H., Breton, C., Moravcoca, J. & Imberty, A. (2003). *Glycobiology*, **13**, 377–386.

Lazar, K. & Walker, S. (2002). *Curr. Opin. Chem. Biol.* **6**, 786–793.

Liu, J. & Balasubramanian, M. K. (2001). *Curr. Drug. Targets Infect. Disord.* **1**, 159–169.

Marcus, S. L., Polakowski, R., Seto, N., Leinala, E., Borisova, S., Blancher, A., Roubinet, F., Evans, S. V. & Palcic, M. M. (2003). *J. Biol. Chem.* **278**, 12403–12405.

Murshudov, G. N., Vagin, A. A. & Dodson, E. J. (1997). *Acta Cryst.* D**53**, 240–255.

Patenaude, S. I., Seto, N. O. L., Borisova, S. N., Szpacenko, A., Marcus, S. L., Palcic, M. M. & Evans, S. V. (2002). *Nature Struct. Biol.* **9**, 685–690.

Pflugrath, J. W. (1999). *Acta Cryst.* D**55**, 1718–1725.

Qasba, P. K., Ramakrishnan, B. & Boeggeman, E. (2005). *Trends Biochem. Sci.* **30**, 53–62.

Seto, N., Compstone, C. A., Evans, S. V., Bundle, D. R., Narang, S. A. & Palcic, M. M. (1999). *Eur. J. Biochem.* **259**, 770–775.

Somsak, L., Nagya, V., Hadady, Z., Docsa, T. & Gergely, P. (2003). *Curr. Pharm. Des.* **9**, 1177–1189.

Tatusova, T. A. & Madden, T. L. (1999). *FEMS Microbiol. Lett.* **174**, 247–250.

Unligil, U. M., Zhou, S., Yuwaraj, S., Sarkar, M., Schachter, H. & Rini, J. M. (2000). *EMBO J.* **19**, 5269–5280.

Vagin, A. & Teplyakov, A. (1997). *J. Appl. Cryst.* **30**, 1022–1025.

Yamamoto, F., Clausen, H., White, T., Marken, J. & Hakomori, S. (1990). *Nature (London)*, **345**, 229–233.

Yazer, M. H., Olsson, M. L. & Palcic, M. M. (2006). *Transfus. Med. Rev.* **20**, 207–217.

Yazer, M. H. & Palcic, M. M. (2005). *Transfus. Med. Rev.* **19**, 210–216.